ResearchGate

See discussions, stats, and author profiles for this publication at: https://www.researchgate.net/publication/315901244

Non-Catalytic Vapor Growth Regime for Organohalide Peroskvite Nanowire Using Anodic Aluminum Oxide Templates

Article *in* Nanoscale · April 2017

DOI: 10.1039/C7NR00444C

CITATION
1

READS
35

9 authors, including:

Mohammad mahdi Tavakoli
Sharif University of Technology
38 PUBLICATIONS **216** CITATIONS
SEE PROFILE

Aashir Waleed
The Hong Kong University of Science and Tec…
9 PUBLICATIONS **18** CITATIONS
SEE PROFILE

R. Tavakoli
Sharif University of Technology
35 PUBLICATIONS **238** CITATIONS
SEE PROFILE

Zhiyong Fan
The Hong Kong University of Science and Tec…
176 PUBLICATIONS **8,917** CITATIONS
SEE PROFILE

Some of the authors of this publication are also working on these related projects:

3D Nano-spikes based System for Biological Manipulation (electroporation, cell lysis, intracellular content extraction) and Sensing (cancer, bio-molecules) at Low Voltages View project

Perovskite materials (thin film, nanowires, and quantum dots) View project

All content following this page was uploaded by Aashir Waleed on 12 April 2017.

The user has requested enhancement of the downloaded file.

Check for updates

View Article Online
View Journal

Nanoscale

Accepted Manuscript

This article can be cited before page numbers have been issued, to do this please use: M. M. Tavakoli, A. waleed, L. Gu, D. Zhang, R. Tavakoli, B. Lei, W. Su, F. Fang and Z. Fan, *Nanoscale*, 2017, DOI: 10.1039/C7NR00444C.

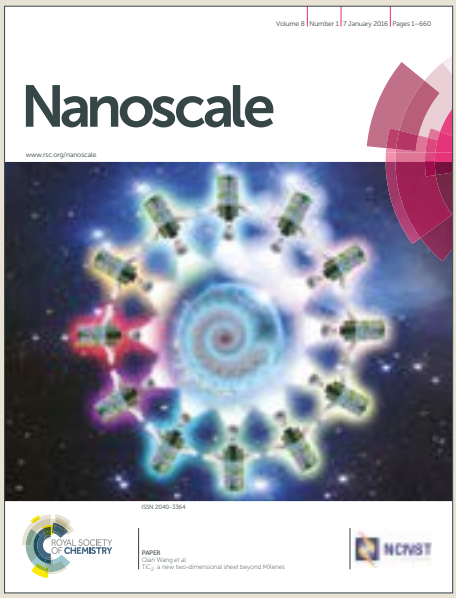

This is an Accepted Manuscript, which has been through the Royal Society of Chemistry peer review process and has been accepted for publication.

Accepted Manuscripts are published online shortly after acceptance, before technical editing, formatting and proof reading. Using this free service, authors can make their results available to the community, in citable form, before we publish the edited article. We will replace this Accepted Manuscript with the edited and formatted Advance Article as soon as it is available.

You can find more information about Accepted Manuscripts in the author guidelines.

Please note that technical editing may introduce minor changes to the text and/or graphics, which may alter content. The journal's standard Terms & Conditions and the ethical guidelines, outlined in our author and reviewer resource centre, still apply. In no event shall the Royal Society of Chemistry be held responsible for any errors or omissions in this Accepted Manuscript or any consequences arising from the use of any information it contains.

ROYAL SOCIETY OF CHEMISTRY

rsc.li/nanoscale

Please do not adjust margins

View Article Online
DOI: 10.1039/C7NR00444C

ARTICLE

Non-Catalytic Vapor Growth Regime for Organohalide Peroskvite Nanowire Using Anodic Aluminum Oxide Templates

Received 00th January 20xx,
Accepted 00th January 20xx

DOI: 10.1039/x0xx00000x

www.rsc.org/

Mohammad Mahdi Tavakoli[a], Aashir Waleed[a,b], Leilei Gu[a], Daquan Zhang[a], Rouhollah Tavakoli[c], Bingbing Lei[d], Wenjun Su[e], Fang Fang[d,*], Zhiyong Fan[a,*]

In this work, a novel and facile synthesis process to fabricate single crystalline organometal halide perovskite nanowires was successfully developed. The nanowires were grown in high density ordered array from metal nanoclusters inside anodic aluminum oxide templates using non-catalytic chemical vapor deposition method. Specifically, the perovskite NWs were grown as a result of the reaction between methylammonium iodide (MAI) and the Pb/Sn (Pb or Sn) metal in anodic aluminum oxide templates under optimal conditions. The characterization results show that there is a reaction zone at the interface between perovskite material and metal, at the bottom of the anodic aluminum oxide nanochannels. In order to sustain perovskite NW growth, MAI molecules have to diffuse downward through the perovskite NWs to reach the reaction zone. In fact, the reaction is facilitated by formation of the intermediate product of metal iodide compound. This suggests that the Pb/Sn metal is converted to PbI_2/SnI_2 first and then perovskite NWs are formed as a result of the reaction between the MAI and PbI_2/SnI_2 through a Vapor-Solid-Solid process. The optical characterization results demonstrate that the as-synthesized NWs with ultra-high nanostructure density can serve as ideal candidates for optoelectronic device, such as solar cells, light-emitting didoes, photodetectors, and *etc*. And the reported growth approach here is highly versatile combining the merits of excellent controllability, cost-effectiveness and tunability on material composition and physical properties.

Introduction

The emergence of high performance organometal halide perovskite materials has been regarded as an important breakthrough in the field of optoelectronic material, owing to their appealing physical properties such as direct energy band gap, high optical absorption coefficient, high charge-carrier mobility, and long carrier diffusion length up to 175 μm.[1-4] Conventionally, thin film perovskite materials have been used widely for solar cells,[5] light-emitting diodes,[6] *etc*., meanwhile a number of synthesis approaches have been developed over the past few years to fabricate single crystal perovskites with different shapes, including quantum dots (QDs)[7], nanowires (NWs),[8-10] and nanosheets,[11] etc. Particularly, perovskite NWs have attracted great deal of interest due to their unique dimension and intriguing optical and electrical properties. More importantly, NW structures can be used for a variety of high performance and integrated devices including transistors, diodes, photodetectors, chemical sensors and so on, which have been widely reported for inorganic semiconducting materials previously.[12] Typically each individual perovskite NW is monocrystalline, resulting in a longer carrier diffusion length and higher charge mobility, compared to polycrystalline thin film perovskite.[13-17] The synthesis of perovskite NWs using a low-temperature process such as solution method is advantageous; however, this material is unstable inside polar inorganic solvent and easily decomposed in this type solvent, resulting in poor crystalinity of NWs.[13] There have been several research groups reported fabrication of perovskite NWs using solution processes.[9-12] For examples, the researchers have used lead acetate as a Pb precursor to synthesize high quality perovskite NWs with lower defect density.[18-21] In particular, Jin *et al*.[10] have proposed a low-temperature (80 ºC) and catalyst-free approach for the fabrication of perovskite NWs using lead acetate precursor and reported that the perovskite NWs were grown along the axis of screw dislocations in the seed layer. In addition, Zhu *et al*.[22] fabricated perovskite NWs using spin coating of Dimethylformamide (DMF)/Isopropyl alcohol (IPA) solvent on top of perovskite film, followed by proper annealing. As a matter of fact, vapor phase processes, *i.e.*, vapor–liquid–solid (VLS) and vapor–solid–solid (VSS) processes, which require metal nano-droplets as catalysts, have been widely used for inorganic NW growth in the past as these processes can yield monocrystalline high quality NWs.[23-25] However, up-until-now, using these approaches to fabricate perovskite NWs have not been widely explored due to very different nature of organometals as compared with inorganic materials, except for indirect method to covert PbX_2 (Br, I) NWs to $MAPbX_3$ NWs in vapor phase.

[a]*Department of Electronic and Computer Engineering, Hong Kong University of Science and Technology, Clear Water Bay, Kowloon, Hong Kong SAR, China*
[b]*Department of Electrical Engineering, University of Engineering and Technology, Lahore (FSD Campus), 3.5 km, Khurrianwala-Makuana Bypass, Faisalabad, 38000, Pakistan*
[c]*Department of Materials Science and Engineering, Sharif University of Technology, Tehran, Iran*
[d]*Department of Materials Science, Fudan University, Shanghai 200433, China*
[e]*School of Mechanical Engineering, Xi'an Jiaotong University, Xi'an, Shaanxi 710049, China*
*Contact details: eezfan@ust.hk (Z. Fan); f_fang@fudan.edu.cn (F. Fang)
Electronic Supplementary Information (ESI) available: SEM images, EDAX mapping, XRD pattern, and optical measurements See DOI: 10.1039/x0xx00000x

Published on 31 March 2017. Downloaded by HK University of Science and Technology on 12/04/2017 12:41:03.

Nanoscale Accepted Manuscript

Published on 31 March 2017. Downloaded by HK University of Science and Technology on 12/04/2017 12:41:03.

View Article Online
DOI: 10.1039/C7NR00444C

Herein, we developed a novel and facile VSS process to fabricate perovskite NWs inside the anodic alumina oxide (AAO) templates using chemical vapor deposition (CVD) method. With this method, we have reported high density three-dimensional (3-D) array of perovskite NWs with precisely controlled geometry.[12] These NWs have promising potency for highly integrated nanoelectronics and optoelectronics. In this work, we performed a systematic study to achieve better understanding on the NW growth kinetics. Particularly, growth of crystalline Pb and Sn based perovskite NWs were investigated using the VSS process, the perovskite NWs (solid) were formed after the reaction of MAI vapor with Pb/Sn precursors (solid) at the bottom of the AAO channels. The results of the characterization indicate that there is an intermediate compound (PbI_2 or SnI_2) inside the reaction zone located at the interface between perovskite NW and metal precursor during the synthesis of perovskite NWs. Moreover, to drive the continuous growth of perovskite NWs, MAI molecules need to diffuse downward through the solid NWs to reach the reaction zone. In addition, the optical properties of the as-synthesized perovskite NWs with ultra-high nanostructure density shows that these single crystal NWs are excellent candidates for optoelectronic devices. Moreover, using our technique, it is possible to tune the composition of perovskite NWs by doping different halides (Cl, Br, and I) in different growth steps.

Results and discussion

Figure 1 shows the schematic of CVD process and growth steps of organometal halide perovskite NWs. In order to synthesize Pb/Sn perovskite NWs, first the metal precursor (Pb/Sn) was electrodeposited inside the one-end-opened AAO channels.

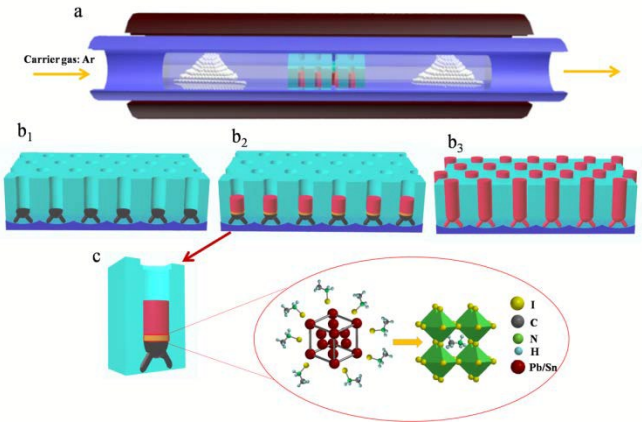

Figure 1. (a) Schematic of a CVD process for perovskite NW growth; (b_1) Pb/Sn metal inside the AAO membrane before reaction; (b_2) Incomplete growth of perovskite NWs in the membrane; (b3) Pb/Sn perovskite NWs inside the AAO membrane after reaction; and (c) Incomplete growth of one individual NW with the details of the reaction.

The amount of metal inside the AAO was controlled by the electrochemical deposition time, as shown in the graph of Figure S1. Afterward, the chip was placed at the center of a tubular CVD furnace inside a secondary glass tube right next to MAI power, as shown in Fig. 1a. The secondary glass tube consists a pair of glass test tubes with the open end facing each other. With this configuration, MAI vapor can be efficiently trapped inside the glass tube to ensure fast NW growth. During NW growth, continuous argon gas flow was supplied to maintain an inert reaction environment. The details of Pb/Sn perovskite nanowires fabrication process is described in experimental section. The schematic of growth procedure for perovskite NWs is shown in Figure $1b_1$-$1b_3$. As it can be seen, this process requires an optimal amount of metal precursor inside the AAO channel to grow NWs with the same height of AAO template (depending on the height and diameter of the channels). It is noteworthy that this is a non-catalytic growth mechanism because the metal precursor has to be consumed completely after the growth process. During the NW growth, the MAI molecules diffuse into the AAO nanochannels with argon as a carrier gas and then reacts with metal to form the perovskite NWs, as shown in Fig. 1c. As it is illustrated, there is a reaction zone at the interface between the metal and perovskite zones. In this region, two reactions occur leading to formation of perovskite NWs, as shown in formula 1 and 2 below. The overall combined reaction is shown in formula 3.

$$2CH_3NH_3I + Pb/Sn \rightarrow Pb/SnI_2 + 2CH_3NH_2 + H_2 \quad (1)$$

$$Pb/SnI_2 + CH_3NH_3I \rightarrow CH_3NH_3Pb/SnI_3 \quad (2)$$

$$3CH_3NH_3I + Pb/Sn \rightarrow CH_3NH_3Pb/SnI_3 + 2CH_3NH_2 + H_2 \quad (3)$$

According to reaction 1, Pb/Sn metal reacts with MAI molecules resulting in PbI_2/SnI_2 compound. Then, perovskite NWs are grown as a result of the reaction between PbI_2/SnI_2 and MAI inside the AAO membrane. The optimal reaction time depends on the temperature, amount of MAI source, and flow rate. As shown in Fig. 1c, the Pb/Sn atoms cannot migrate upward through the perovskite NW bulk due to its high density and lower diffusion constant.[30] Consequently, in order to complete the reaction, the MAI molecules with high mobility diffuse through the solid perovskite NWs to reach the reaction zone and followed by the reaction 1 and 2, which is driven by the elevated temperature. Essentially, this process is a vapor-solid-solid (VSS) process which is based on the downward diffusion mechanism of MAI molecules and the reaction rate can be controlled by flow rate and temperature.

Interestingly, the reaction between the Pb/Sn metal and MAI leads to a large volume increase. Note that lead and white tin are face-centered-cubic (FCC) with 4 atoms and body-centered-tetragonal (BCT) with 2 atoms in a unit cell, respectively. Since each crystal unit cell of perovskite material needs only one Pb/Sn atom, one Pb and Sn crystal unit cell can evolve into 4 and 2 perovskite lattice unit cells at the end of the growth process, respectively. According to the literature[27,28], the lattice constants of perovskite, Pb, and Sn are 629 pm, 492 pm, and 583×583×318 pm, respectively. As a result, by using a simple calculation (equation 4), the volume increase ratio for the fabrication of the perovskite NWs from Pb and Sn metals are 8.35 and 4.6, respectively:

$$Volume\ increase\ ratio = \frac{4(2)\times V_{MAPb/SnI3}}{V_{Pb/Sn}} \quad (4)$$

Where $V_{MAPb/SnI3}$ and $V_{Pb/Sn}$ are the volumes of $MAPb/SnI_3$ and Pb/Sn lattice unit cells, respectively. Consequently, the amount of Pb/Sn metal inside the AAO channels needs to be controlled by the electrodepostion time in order to completely fill the AAO membrane by perovskite NWs. Figure 2 shows the SEM images of as-grown

Nanoscale Accepted Manuscript

View Article Online
DOI: 10.1039/C7NR00444C

Published on 31 March 2017. Downloaded by HK University of Science and Technology on 12/04/2017 12:41:03.

perovskite NWs. Specifically, Fig. 2a_1-a_4 show the cross sectional SEM images of AAO before NW growth (2a_1) and after 20 min (2a_2), 40 min (2a_3), 80 min (2a_4) NW growth. These images reveal that the perovskite NWs growth involves a non-catalytic reaction between Pb metal and MAI molecules, without metal catalyst capping the NWs as seen in the inorganic Vapor-Liquid-Solid NW growth.[29] And due to the large volume increase from metal to perovskite material after the reaction, the NWs may come out from the confined AAO channels. The growth steps of Sn perovskite NWs are also shown in Figure S2. Figure 2b, c shows the top-view SEM images of Pb and Sn perovskite NWs with a completed filling ratio and highly crystalline structure. As seen, the diameter of NWs is in a range of 70-250 nm. To explore the composition of perovskite NWs after the reaction, energy-dispersive x-ray (EDAX) mapping is acquired on the cross section of a Pb perovskite NW array. As shown in Figure S3, the NWs showed a uniform elemental distribution of Pb, I, and C. It is worth pointing out that in our proposed method the geometry of perovskite NWs can be easily tuned by template engineering. Figure S4 show top and cross-sectional views of nanowells with diameter of less than 100 nm before and after growth of Pb perovskite NWs. This suggests that our approach is versatile to fabricate an array of NWs with different diameters and heights. In order to further study the role of AAO on fabrication of perovskite NWs, the same experiment was performed to grow NWs using Pb metal film deposited on glass substrate. As shown in Figure S5, the Pb NWs are grown from Pb film with a very low density and poor order. Furthermore, the diameter and height of NWs are out of control in this case.

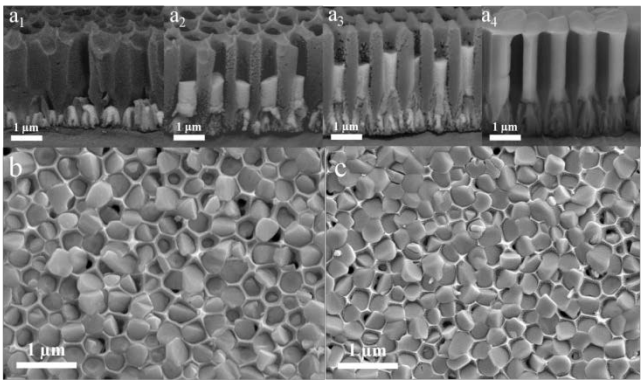

Figure 2. (a_1-a_4) Cross-sectional SEM images of the AAO membrane, showing Pb metal before and after reaction at different growth times. Top-view SEM images of (b) Pb, and (c) Sn perovskite NWs inside the AAO membrane.

To further study the reaction between Pb/Sn metal and MAI, we measured the thermal behavior of MAI by using thermogravimetric analysis (TGA) and differential scanning calorimetry (DSC) tests. Figure 3a shows the TGA curve (blue curve) of MAI, indicating its mass loss behavior, which started at ~70ºC. As it can be seen, the weight loss is accelerated by increasing the temperature. Also, the first derivative curve (purple curve) demonstrates that the mass loss increases drastically at temperatures higher than 180 ºC, which suggests the proper temperature for the formation of perovskite NWs. Figure 3b shows the DSC plot of the MAI powder, showing the rock-salt to the ionic plastic phase transition at around 140 to 150 ˚C. Additionally, the phase of MAI changes to ε-MAI above 150 ºC.[26] In fact, this phase has a higher sublimation rate.[30] Since the MAI vaporization is poor below this temperature, we have studied the mass loss of MAI at different temperatures (150, 165, and 180 ºC) *versus* time (Figure 3c). The results illustrate that below 180 ºC, the reaction is slow due to the low vapor pressure of MAI. Beside thermal analysis of the MAI powder, we studied the composition of NWs after growth inside the AAO channels using time-of-flight secondary ion mass spectrometry (TOF-SIMS), as shown in Figures 3d, e and S6. In this experiment, two AAO samples with different amounts of lead were prepared, and after complete the reaction, TOF-SIMS analysis was performed for as-synthesized perovskite NWs. Dual beam TOF-SIMS depth profiling was employed to detect the distribution of basic elements through the length of the NWs.

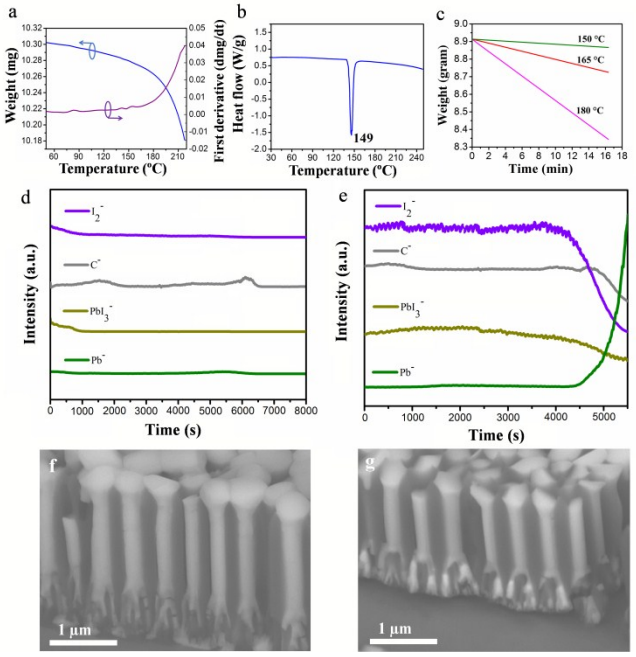

Figure 3. (a) TGA heating and its first derivative curves; (b) DSC heating curve of MAI powder; and (c) thermogravimetric analysis of MAI at 150, 165, and 180ºC. ToF-SIMS profiles and backscattered SEM images of Pb perovskite NWs inside the AAO membrane with (d,f) optimum, and (e,g) extra amount of Pb.

Figure 3d shows the TOF-SIMS profile of the sample with a completed reaction, uniform distribution of elements, and sufficient amount of Pb at the bottom. In addition, Figures 3d and 3e show TOF-SIMS analysis for another NWs sample with a large amount Pb and the same growth conditions, which correspond to SEM images of as-grown perovskite NWs inside AAO channels (Figures 3f and 3g). As illustrated in Figure 3e, the TOF-SIMS profile shows that there is still extra amount of Pb at the bottom of the AAO channels after growth. Moreover, the amount of other compounds at the end of the channels is decreased, as shown in Figure 3e. This suggests that the reaction time and the amount of Pb at the bottom of the AAO channels have to be controlled precisely, in order to have a uniform composition for perovskite NWs. More interestingly, it was discovered that Pb metal stays at the bottom of the channels during the reaction. Thus, there must be a downward solid-state diffusion process for MAI molecules through the perovskite NWs to reach the Pb metal and complete the reaction continuously, as shown in Figure 1d. In addition, the TOF-SIMS profile was performed for Sn perovskite NWs as well, and as shown in Figure S6, there is a

Nanoscale Accepted Manuscript

View Article Online
DOI: 10.1039/C7NR00444G

Published on 31 March 2017. Downloaded by HK University of Science and Technology on 12/04/2017 12:41:03.

uniform distribution of elements for tin perovskite through the length of the NWs after optimization of the growth conditions.

Notably, we proposed that there is a reaction zone at the bottom of the AAO channels in our reaction mechanism. In order to synthesize perovskite NWs from Pb/Sn metal, there are two reactions, as shown in formula 1 and 2. In fact, we mentioned that there is an intermediate compound as the result of formula 1 reaction, *i.e.* PbI_2/SnI_2. In order to confirm this, Pb metal was deposited on the surface of FTO glass. The CVD process with the same conditions as the perovskite NWs was carried out for synthesis of perovskite planar film from the Pb metal layer. Figure 4 shows the top-view SEM images and the photographs of the samples after different reaction times of 0 min, 45 min and 100 min. A Pb film with island-like microstructures is shown in Figure 4a. After running the CVD process at 180 ºC for 20 min, the color of the sample became yellowish and its top-view SEM confirms that this is PbI_2 film with a hexagonal shape on the surface, as shown in Figure 4b. Thereafter, the reaction was continued and completed for 1 h, resulting in a sample with a brownish color and a highly crystalline perovskite film, as illustrated in Figure 4c. In order to support the proposed two step growth mechansim, XRD patterns of these films (Figs. 4a-c) were measured. The results indicate that XRD peaks of the films shown in Figures 4a, 4b, and 4c correspond to Pb, PbI_2, and Perovskite films, respectively. This suggests that there is an intermediate state during the reaction, which should be the same for perovskite NW growth as well.

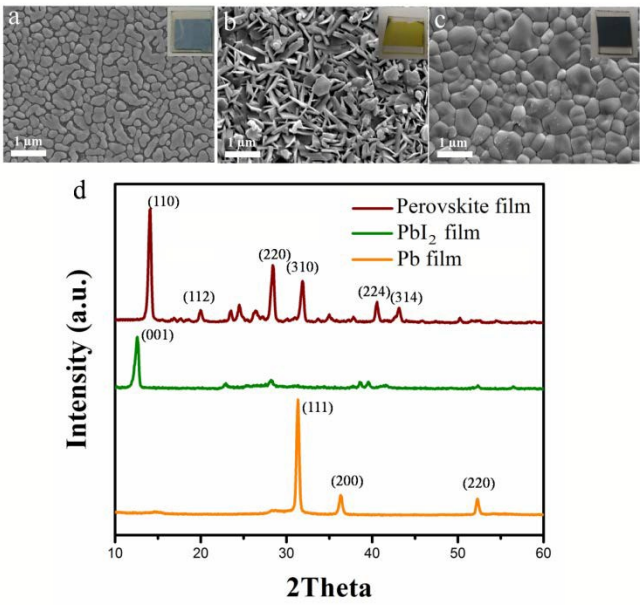

Figure 4. Top-view SEM images and micrographs of (a) electrodeposited Pb metal on FTO glass; (b) PbI_2 film prepared by the short reaction of Pb metal and MAI; and (c) Pb perovskite film with a highly crystalline structure after the completed the reaction. (d) XRD patterns of the samples corresponding to the figures (a) Pb, (b) PbI_2, and (c) perovskite film during the reaction.

One of the controlling parameters for the NW length is the amount of Pb/Sn metal inside the AAO channels. According to the above calculation, Pb/Sn perovskite NWs have an 8.35 and 4.6 times volume increase from metal precursors after the reaction. Thus, by increasing the amount of Pb/Sn metal and controlling the growth conditions, the NWs could grow out of the AAO channels, as shown in Figure S7. The cross-sectional SEM image of perovskite NWs in back-scatter electron (BSE) mode shows that there is a small area with a bright color at the end of the AAO channels, thus showing the extra amount of Pb after the reaction. This proves that the Pb/Sn metal remains at the bottom of membrane and there is a downward diffusional mechanism for MAI molecules to complete the perovskite reaction. Meanwhile, besides the amount of Pb/Sn metal, the reaction temperature is another key parameter to grow the NWs out of the AAO membrane. In this regard, we found that the temperature range for growth of NWs is 160-170 ºC. It is worth pointing out that by increasing the reaction temperature to more than 180 ºC, the perovskite NWs at the top of the AAO merge into each other and form a perovskite film due to coalescence and grain coarsening phenomena. This results in a highly crystalline perovskite film with large grain size on top of the AAO membrane, as shown in Figure S8. In addition, if all of the metal inside the channels was consumed after a long reaction time, the perovskite NWs could be decomposed from the top due to high temperature and lack of a metal source for reaction.

The results of characterizations for Pb/Sn perovskite NWs are shown in Figure 5 and S9. Figure 5a shows the tilted angular view SEM image of Pb perovskite NWs, which were grown outside of the AAO membrane. XRD patterns of pure Pb/Sn metal inside the AAO channels before and after reactions are displayed in Figures 5b and S9, respectively. As it can be seen, the Pb/Sn metals have been completely converted to highly crystalline Pb/Sn perovskite NWs without impurity and there is not any peak related to Pb/Sn metal and PbI_2/SnI_2 compound after the reaction. Moreover, the XRD patterns of NWs show a set of strong peaks, which correspond to the cubic crystal structure of CH_3NH_3Pb/SnI_3.

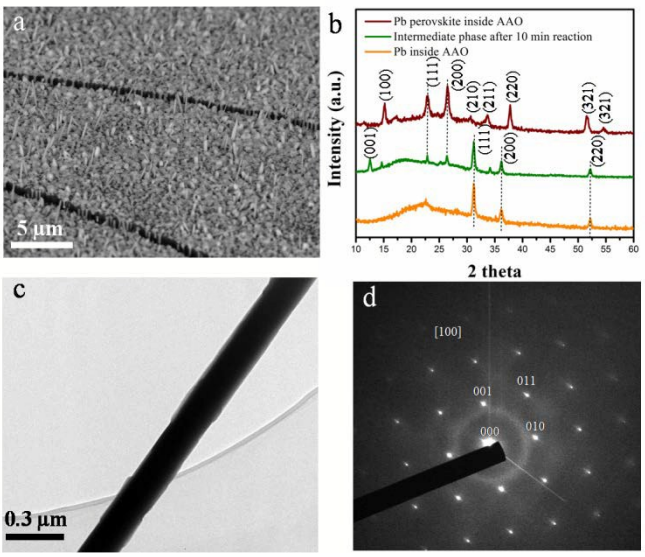

Figure 5. (a) Top-view SEM image of Pb perovskite NWs which have been grown out of the channels; (b) XRD patterns of Pb metal, intermediate phase after 10 min reaction, and Pb perovskite NWs inside the AAO membrane; (c) TEM image of an individual NW transferred to the TEM grid; and (d) SAED pattern of one individual Pb perovskite NW.

In addition, we grew perovskite NWs inside the AAO template and run the CVD process for only 10 min. The XRD result of this sample

Nanoscale Accepted Manuscript

Published on 31 March 2017. Downloaded by HK University of Science and Technology on 12/04/2017 12:41:03.

View Article Online
DOI: 10.1039/C7NR00444C

(Figure 5b) shows that besides the Pb metal and perovskite peaks, there is a strong peak located at 12.6º, indicating the presence of the PbI_2 phase inside the AAO channels.[15] This suggests that PbI_2 is an intermediate phase in this growth technique even inside AAO channels. In order to investigate the crystalline quality of the perovskite NWs, they were transferred to a TEM grid (Figure 5c). The selected-area diffraction pattern (SAED) of Pb perovskite NW is shown in Figure 5d. As it can be seen, the clearly resolved bright spots in the diffraction pattern suggest a single crystal NW with a cubic structure and preferential growth direction of [100]. In order to support this claim, more SAED patterns from the same NW shown in Figure 5c and another individual NW were taken, as shown in Figure S10. In fact, the SAED patterns shown in Figure 5d and S10a were taken from one individual Pb perovskite NW, which indicate that the NW is single crystal with a crystal direction of [100]. Figure S10b shows SAED pattern of another individual sigle crystal Pb perovskite NW with a crystal direction of [111]. The SAED patterns and XRD results suggest that using AAO template, the individual Pb perovskite NWs are grown in different crystal directions.

Besides the crystal structure of NWs, their optical properties have also been studied using UV-Visible and photoluminescence (PL) measurements. Figure 6a and S11 demonstrate the optical absorption and PL spectra of Pb and Sn perovskite NWs, respectively. Since the AAO membrane is transparent with a large band gap, the results reflect the intrinsic properties of NWs. The optical absorption spectra of Pb and Sn perovskite NWs indicate an optical band gap of 1.57 eV and 1.3 eV, respectively. Furthermore, the sharp excitonic peaks in the PL spectra of Pb and Sn perovskite NWs, located at 790 nm and 950 nm, respectively, are consistent with the absorption measurement results, indicating the excellent optical properties of theses NWs, which will find applications for high performance optoelectronic devices. Meanwhile, the time-resolved PL measurement of Pb perovskite NWs shows an estimated carrier life-time of 32.1 ns, which is better than $CH_3NH_3PbI_3$ thin film (~10 nm)[3], as shown in Fig. 6b and Table S1. This result confirms the desirable quality of NWs fabricated using this process.

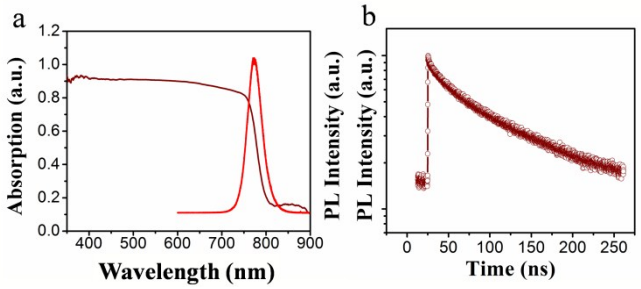

Figure 6. The optical properties of Pb perovskite NW array inside the AAO membrane, (a) UV-visible and PL spectra; (b) Time-resolved PL curve of the sample.

In order to evaluate the stability of perovskite NWs inside the AAO channel, we have designed a control experiment using Sn perovskite NWs as an example. Here, we have measured the PL spectrum of NWs inside the AAO over time to test the stability. These results have been compared with Sn perovskite thin film deposited with thermal evaporation. Figure S12 shows the PL spectra of NWs and thin film Sn perovskite right after growth, after 1 day, and after 8 days maintaining in the dry-box (20% humidity). Interestingly, it was found that AAO template dramatically improves Sn perovskite NWs stability. As it is seen, the PL intensity of NWs sample drops only 5% and 45% after 1 day and 8 days kept in the dry-box, respectively, indicating much improved stability of NWs by AAO template passivation. In contrast, the PL intensity of Sn perovskite thin film completely disappear after one day, showing its poor stability.

Conclusions

In this work, we demonstrate a novel vapor phase synthesis process to fabricate Pb/Sn perovskite NWs arrays with a well-control of NW dimensions, crystallinity, and composition. It was shown that this is a non-catalytic growth mechanism for Pb/Sn perovskite NWs, which is distinctly different from the previous reports on most inorganic NW growth processes. Herein, arrays of Pb/Sn perovskite NWs were grown directly from the Pb/Sn metal precursor inside the AAO channels by using CVD process. Essentially, the NWs were grown as a result of the reaction between Pb/Sn metal and MAI. The characterization results indicate that there is an intermediate product in the synthesis process from Pb/Sn metal to perovskite NWs, namely, the metal precursor needs to be converted to PbI_2/SnI_2 followed by the subsequent reaction. The results of ToF-SIMS, XRD and SEM images confirm that there is a reaction zone at the bottom of the AAO channels and MAI has to diffuse downward through the solid perovskite NWs to reach the metal precursor in order to continue the reaction. The optical measurement results of perovskite NWs show that the as-synthesized NWs are an excellent candidate for optoelectronics. Overall, compared with the methods already reported in the literature, our unique perovskite NW fabrication process can enable a new, facile and generic synthesis process for a wide variety of organometal perovskite nanostructures beyond NWs, due to the unique template confinement. The excellent controllability on the material geometry (diameters and height of NWs) adds up to great flexibility for various optoelectronic device structure designs. And the ultra-high nanostructure density with a good alignment may lead to applications for highly integrated electronics and optoelectronics with organometal perovskite materials. Finally, a drastically improved stability of NWs using AAO template makes the reported NW growth method more attractive than other alternative NW growth approaches.

Experimental

Fabrication of AAO templates and barrier thinning process

To fabricate the AAO templates, a two-step anodization of aluminum foil was used as can be found elsewhere. Briefly, before anodization, an acidic solution (a mixture of 25 vol% $HClO_4$ and 75 vol% absolute CH_3CH_2OH) was employed to electro-polish the aluminum foil using a 10 V direct current (DC) voltage for 2 min. Then, the first anodization process was performed in an aqueous solution (33 vol % ethylene glycol and 0.3 vol % H_3PO_4 (85 wt. % in H_2O)) for 12 h under 200 V to oxidize the chips. Afterward, the anodized Al_2O_3 layer was etched away using an aqueous solution of 6 wt % H_3PO_4 and 1.8 wt % CrO_3 at 98ºC for 30 min. Next, the chips were anodized in the same aqueous solution for 45 min again, followed by etching the chips in a 5 wt% H_3PO_4 aqueous solution at 52 ºC for 10 min to enlarge the channel diameter to ~250 nm.

Electrodeposition of metal precusors (Pb/Sn)

Nanoscale Accepted Manuscript

Published on 31 March 2017. Downloaded by HK University of Science and Technology on 12/04/2017 12:41:03.

To facilitate the electrodepostion, a barrier thinning process was performed by a current ramping process (-3.2 nA/min) to open the barrier layer at the bottom of the AAO channel up to several nanometers. In this report, we used the 1 μm-thick AAO with a 300 nm-thick sub-channel layer to study the growth mechanism.

The electrodeposition (ED) of a Pb/Sn catalyst was carried out using an aqueous solution (70 g/L $PbCl_2$/$SnCl_2$ and 42 g/L tri-sodium citrate (buffer)) inside the AAO template. The ED process was performed for 5 min at room temperature under 6.5 V using the sinuous mode to fill ~300 nm of depth of the AAO sub-channels.

Synthesis of MAI powder

CH_3NH_3I powder was synthesized by slowly mixing 27.8 mL of methylamine (33% wt in ethanol, Sigma Aldrich) and 30 mL of hydroiodic acid (57 wt% in water, Sigma Aldrich) inside a three-neck flask placed in an ice bath with stirring. The MAI powder was precipitated after removing the solvent at 50 °C using a rotary evaporator (Buchi R215, Switzerland). Then, the final product was dissolved in ethanol and precipitated by adding diethyl ether several times. Finally, the powder was dried at 80 °C in a vacuum oven for 24 h.

Fabrication of Pb/Sn perovskite nanowires

In order to fabricate the Pb/Sn perovskite NWs, a tubular CVD furnace (1 inch quartz tube) was employed. After electrodeposition of Pb/Sn metal inside the AAO channels, the chip and MAI powder were put into two-quartz containers at the center of the CVD furnace close to the thermocouple. The reaction between the metal and MAI was performed inside the closed container using argon carrier gas at 180 ºC for 3 h. The distance between the substrate and MAI source was 3 cm, and the flow rate was fixed at 600 sccm.

Characterizations

The samples were characterized using field-emission scanning electron microscopy (JEOL JSM-7100F) equipped with energy-dispersive X-ray spectroscopy (EDS) and X-ray diffraction (Bruker D8 X-ray diffractometer, USA) utilizing Cu *Kα* radiation to study the length, crystallinity, and morphology of the NWs. The optical absorption and steady-state photoluminescence spectra were measured using a Varian Cary 500 spectrometer (Varian, USA) and Edinburgh Instruments FLS920P fluorescence spectrometer, respectively. A high-resolution transmission electron microscope (HRTEM, JEOL-2010F) equipped with an energy-dispersive X-ray spectroscope (EDS) was employed for structural studies. In order to study the MAI reaction and compositional variation of NWs, thermogravimetric analysis (TGA, UNIX/TGA7 (Perkin Elmer)) and a time of flight secondary ion mass spectrometer (ION-TOF GmbH) were utilized, respectively.

Acknowledgements

This work was supported by the General Research Fund (project 612113) from the Hong Kong Research Grant Council, the Hong Kong Innovation and Technology Fund (project ITS/117/13, ITS/362/14FP) from the Innovation and Technology Commission, State Key Laboratory on Advanced Displays and Optoelectronics at HKUST and National Natural Science Foundation of China (project 51672231 and 51471052). Also, the authors would like to thank the support from the Center for 1D/2D Quantum Materials and the State Key Laboratory on Advanced Displays and Optoelectronics at HKUST.

View Article Online
DOI: 10.1039/C7NR00444C

Notes and references

1 S. D. Stranks, G. E. Eperon, G. Grancini, C. Menelaou, M. J. P. Alcocer, T. Leijtens, L. M. Herz, A. Petrozza and H. J. Snaith, *Science* 2013, **342**, 341-344.

2 W. Nie, H. Tsai, R. Asadpour, J. C. Blancon, A. J. Neukirch, G. Gupta, J. J. Crochet, M. Chhowalla, S. Tretiak, M. A. Alam, *et al. Science* 2015, **347**, 522-525.

3 M. M. Tavakoli, L. Gu, Y. Gao, C. Reckmeier, J. He, A. L. Rogach, Y. Yao and Z. Fan, *Sci. Rep.* 2015**, 5**, 14083.

4 M. M. Tavakoli, Q. Lin, S. F. Leung, G.C. Lui, H. Lu, L. Li, B. Xiang and Z. Fan, *Nanoscale* 2016, **8**, 4276-4283.

5 H. J. Snaith, *J. Phys. Chem. Lett.* 2013, **4**, 3623-3630.

6 Y. Ling, Y. Tian, X. Wang, J. C. Wang, J. M. Knox, F. Perez-Orive, Y. Du, L. Tan, K. Hanson, B. Ma and H. Gao, *Adv. Mater*. 2016, **28**, 8983-8989.

7 F. Zhang, H. Zhong, C. Chen, X. G. Wu, X. Hu, H. Huang, J. Han, B. Zou and Y. Dong, *ACS Nano* 2015, **9**, 4533-4542.

8 J. Xing, X. F. Liu, Q. Zhang, S. T. Ha, Y. W. Yuan, C. Shen, T. C. Sum and Q. Xiong, *Nano Lett.* 2015, **15**, 4571-4577.

9 H. Deng, D. Dong, K. Qiao, L. Bu, B. Li, D. Yang, H.E. Wang, Y. Cheng, Z. Zhao, J. Tang, H. Song, *Nanoscale* **2015**, *7*, 4163.

10 H. Zhu, Y. Fu, F. Meng, X. Wu, Z. Gong, Q. Ding, M. V. Gustafsson, M. T. Trinh, S. Jin and X. Y. Zhu, *Nat. Mater.* 2015, **14**, 636-642.

11 J. Liu, Y. Xue, Z. Wang, Z. Q. Xu, C. Zheng, B. Weber, J. Song, Y. Wang, Y. Lu, Y. Zhang and Q. Bao, *ACS Nano* 2016, **10**, 3536-3542.

12 L. Gu, M. M. Tavakoli, D. Zhang, Q. Zhang, A. Waleed, Y. Xiao, K. H. Tsui, Y. Lin, L. Liao, J. Wang and Z. Fan, *Adv. Mater.* 2016, **28**, 9713-9721.

13 A. Fu, P. Yang, *Nat. Mater*. 2015, **14**, 557-558.

14 A. B. Wong, M. Lai, S. W. Eaton, Y. Yu, E. Lin, L. Dou, A. Fu and P. Yang, *Nano Lett.* 2015, **15**, 5519-5524.

15 M. M. Tavakoli, R. Tavakoli, Z. Nourbakhsh, A. Waleed, U. S. Virk and Z. Fan, *Adv. Mater. Interfaces* 2016, **3**, 1500790.

16 D. Zhang, S. W. Eaton, Y. Yu, L. Dou and P. Yang, *JACS* 2015, **137**, 9230-9233.

17 M. M. Tavakoli, K. H. Tsui, Q. Zhang, J. He, Y. Yao, D. Li and Z. Fan, *ACS Nano* 2015, **9**, 10287-10295.

18 S. W. Eaton, M. Lai, N. A. Gibson, A. B. Wong, L. Dou, J. Ma, L. W. Wang, S. R. Leone and P. Yang, *PNAS*, 2016, **113**, 1993-1998.

19 W. Tian, C. Zhao, J. Leng, R. Cui and S. Jin, *JACS* 2015, **137**, 12458-12461.

20 D. Zhang, Y. Yang, Y. Bekenstein, Y. Yu, N. A. Gibson, A. B. Wong, S. W. Eaton, N. Kornienko, Q. Kong, M. Lai and A. P. Alivisatos, *JACS* 2016, **138**, 7236-7239.

21 J. W. Lee, H. S. Kim and N. G. Park, *Acc. Chem. Res.* 2016, **49**, 311-319.

22 P. Zhu, S. Gu, X. Shen, N. Xu, Y. Tan, S. Zhuang, Y. Deng, Z. Lu, Z. Wang and J. Zhu, *Nano Lett.* 2016, **16**, 871-876.

23 S. A. Dayeh, E. T. Yu and D. Wang, *Nano Lett.* 2009, **9**, 1967-1972.

Nanoscale Accepted Manuscript

24 V. G. Dubrovskii, N. V. Sibirev, G. E. Cirlin, I. P. Soshnikov, W. H. Chen, R. Larde, E. Cadel, P. Pareige, T. Xu, B. Grandidier and J. P. Nys, *Phys. Rev. B* 2009, **79**, 205316.
25 D. S. Kim, U. Gösele and M. Zacharias, *J. Cryst. Growth*. 2009, **311**, 3216-3219.
26 Z. Song, S. C. Watthage, A. B. Phillips, B. L. Tompkins, R. J. Ellingson and M. Heben, J. *Chem. Mater*. 2015, **27**, 4612-4619.
27 R. Lamber, S. Wetjen and N. I. Jaeger, *Phys. Rev. B* 1995, **51**, 10968.
28 L. D. Brownlee, *Nature* 1950, **166**, 482.
29 Z. Fan, H. Razavi, J. W. Do, A. Moriwaki, O. Ergen, Y. L. Chueh, P. W. Leu, J. C. Ho, T. Takahashi, L. A. Reichertz and S. Neale, *Nat. Mater*. 2009**, 8**, 648-653.
30 A. Dualeh, P. Gao, S. I. Seok, M. K. Nazeeruddin and M. Grätzel, *Chem. Mater*. 2015, **26**, 6160-6164.

View Article Online
DOI: 10.1039/C7NR00444C

Published on 31 March 2017. Downloaded by HK University of Science and Technology on 12/04/2017 12:41:03.

Nanoscale Accepted Manuscript

View Article Online
DOI: 10.1039/C7NR00444C

Published on 31 March 2017. Downloaded by HK University of Science and Technology on 12/04/2017 12:41:03.

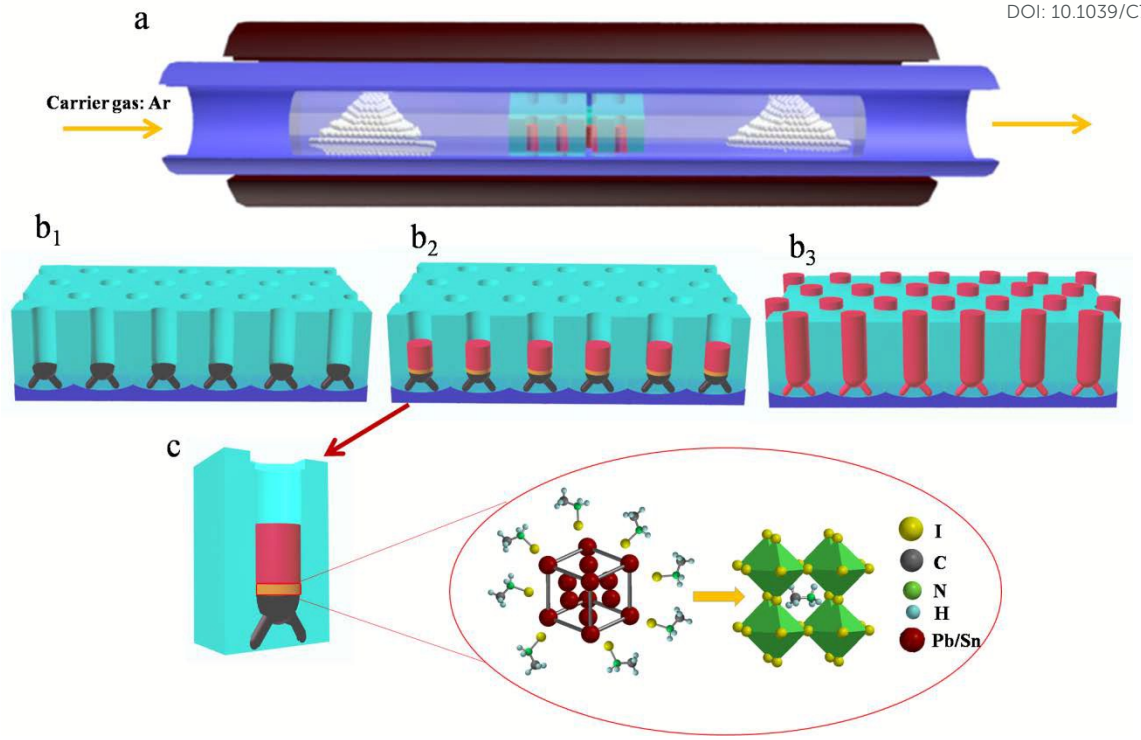

Figure 1. (a) Schematic of a CVD process for perovskite NW growth; (b_1) Pb/Sn metal inside the AAO membrane before reaction; (b_2) Incomplete growth of perovskite NWs in the membrane; (b3) Pb/Sn perovskite NWs inside the AAO membrane after reaction; and (c) Incomplete growth of one individual NW with the details of the reaction.

Nanoscale Accepted Manuscript

View Article Online
DOI: 10.1039/C7NR00444C

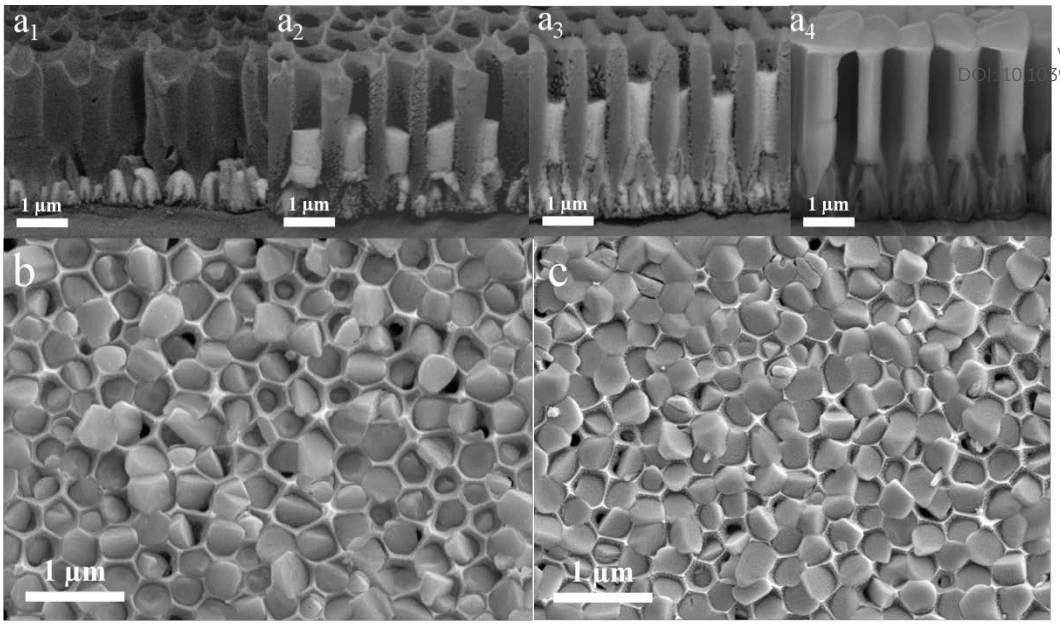

Figure 2. (a_1-a_4) Cross-sectional SEM images of the AAO membrane, showing Pb metal before and after reaction at different growth times. Top-view SEM images of (b) Pb, and (c) Sn perovskite NWs inside the AAO membrane.

Published on 31 March 2017. Downloaded by HK University of Science and Technology on 12/04/2017 12:41:03.

Nanoscale Accepted Manuscript

View Article Online
DOI: 10.1039/C7NR00444C

Published on 31 March 2017. Downloaded by HK University of Science and Technology on 12/04/2017 12:41:03.

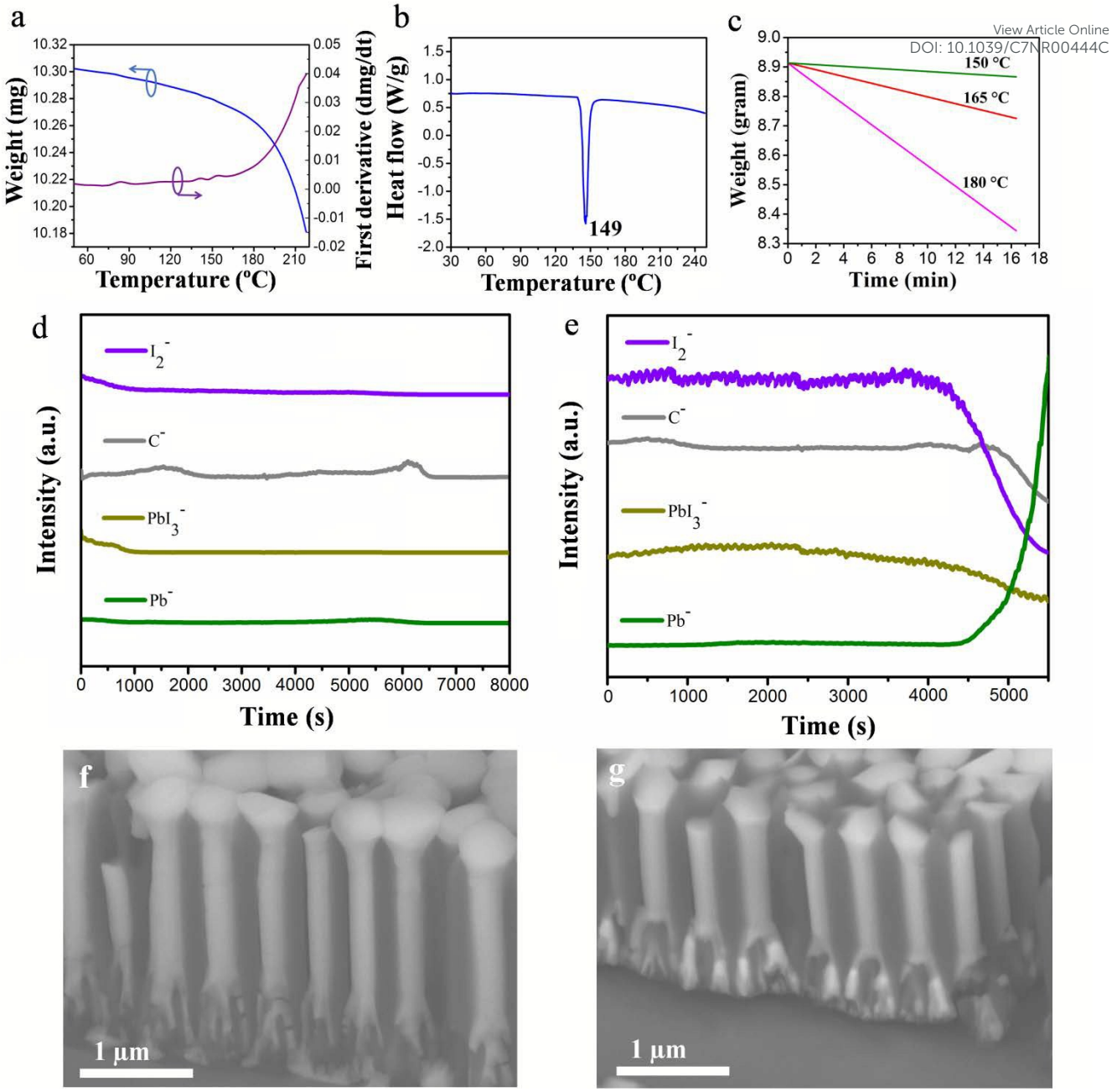

Figure 3. (a) TGA heating and its first derivative curves; (b) DSC heating curve of MAI powder; and (c) thermogravimetric analysis of MAI at 150, 165, and 180ºC. ToF-SIMS profiles and backscattered SEM images of Pb perovskite NWs inside the AAO membrane with (d,f) optimum, and (e,g) extra amount of Pb.

Nanoscale Accepted Manuscript

View Article Online
DOI: 10.1039/C7NR00444C

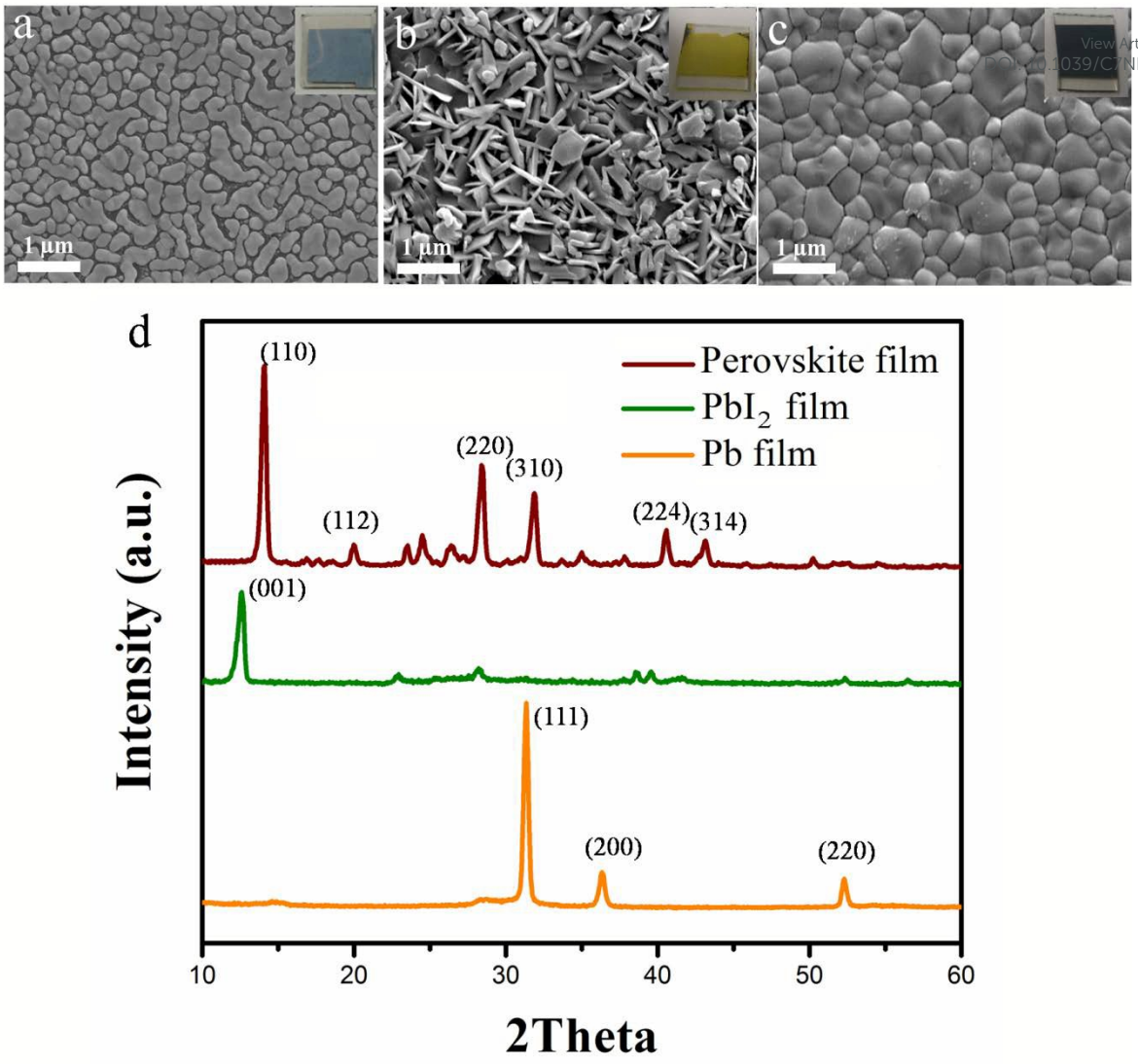

Figure 4. Top-view SEM images and micrographs of (a) electrodeposited Pb metal on FTO glass; (b) PbI_2 film prepared by the short reaction of Pb metal and MAI; and (c) Pb perovskite film with a highly crystalline structure after the completed the reaction. (d) XRD patterns of the samples corresponding to the figures (a) Pb, (b) PbI_2, and (c) perovskite film during the reaction.

Published on 31 March 2017. Downloaded by HK University of Science and Technology on 12/04/2017 12:41:03.

Nanoscale Accepted Manuscript

View Article Online
DOI: 10.1039/C7NR00444C

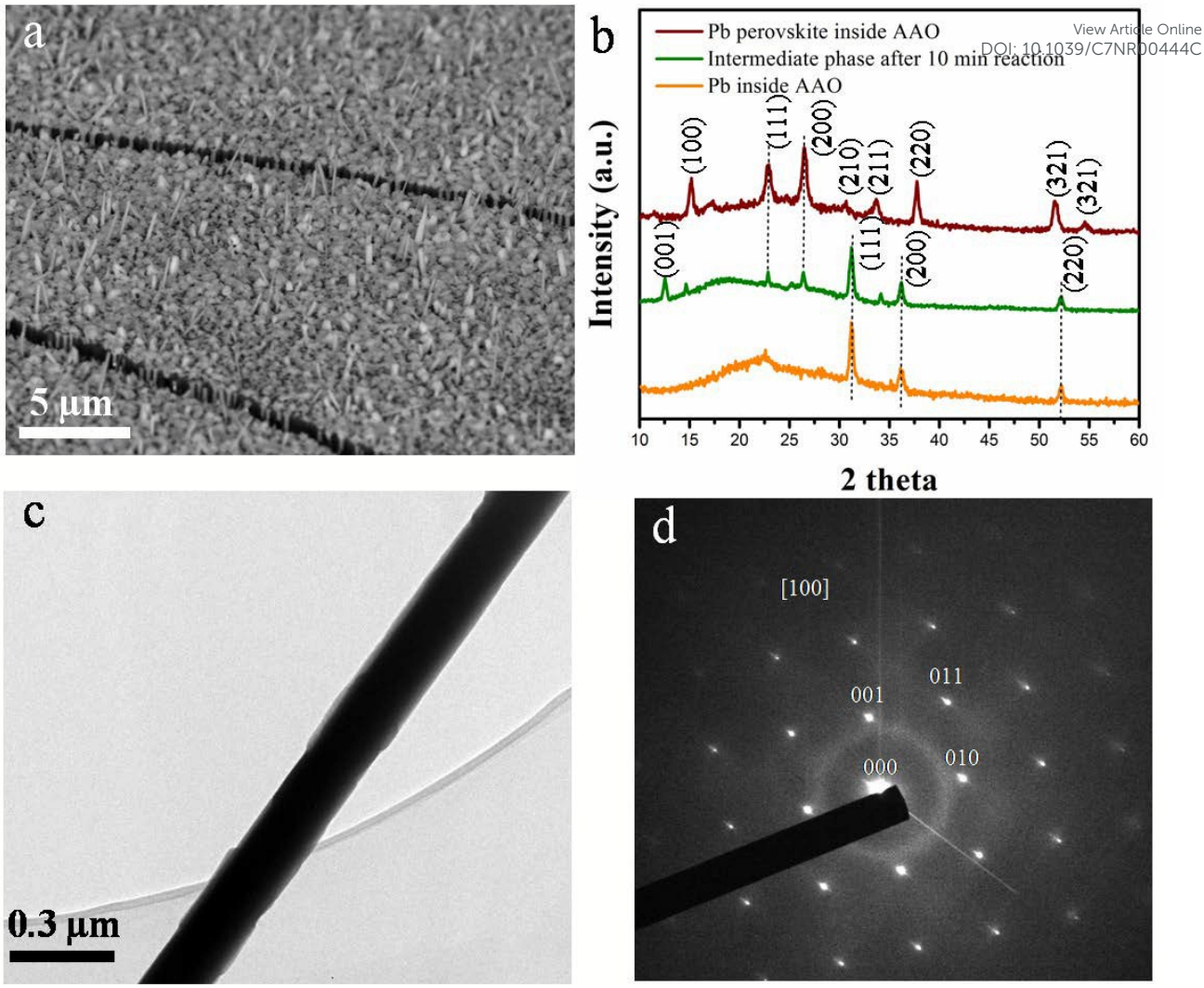

Figure 5. (a) Top-view SEM image of Pb perovskite NWs which have been grown out of the channels; (b) XRD patterns of Pb metal and Pb perovskite NWs inside the AAO membrane; (c) TEM image of an individual NW transferred to the TEM grid; and (d) SAED pattern of one individual Pb perovskite NW.

Published on 31 March 2017. Downloaded by HK University of Science and Technology on 12/04/2017 12:41:03.

Nanoscale Accepted Manuscript

View Article Online
DOI: 10.1039/C7NR00444C

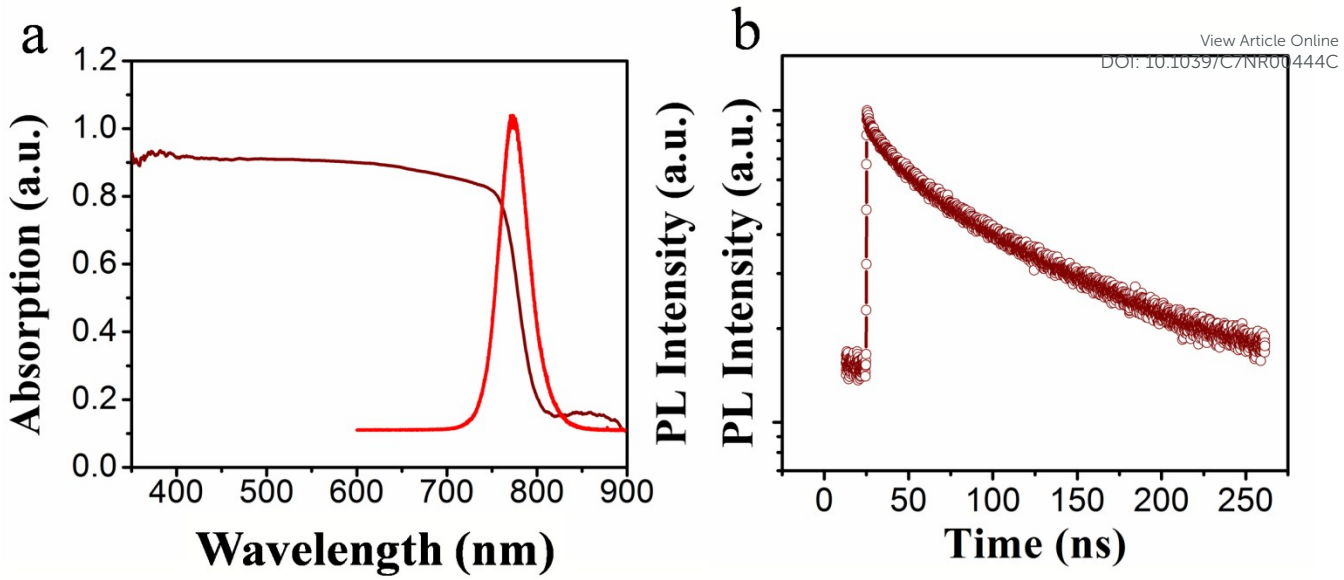

Figure 6. The optical properties of Pb perovskite NW array inside the AAO membrane, (a) UV-visible and PL spectra; (b) Time-resolved PL curve of the sample.

Published on 31 March 2017. Downloaded by HK University of Science and Technology on 12/04/2017 12:41:03.

Nanoscale Accepted Manuscript

View publication stats